

Liquid-diffusion-limited growth of vanadium dioxide single crystals

Nico Sprinkart ^{*}, Daniel Kazenwadel ^{*}, Roman Hartmann , and Peter Baum [†]
Universität Konstanz, Fachbereich Physik, 78464 Konstanz, Germany

 (Received 14 September 2022; revised 12 December 2022; accepted 21 December 2022; published 20 January 2023)

Vanadium dioxide is a strongly correlated material with an ultrafast first-order phase transition between monoclinic/insulator and rutile/metallic close to room temperature. The unusual and complex properties of this transition make VO₂ one of the most heavily investigated materials in modern condensed matter physics. Consequently, high-quality single crystals are in large demand. Here we report the growth of mm-sized VO₂ crystals by thermal decomposition of liquid V₂O₅ at ~1000° C. Time-resolved zirconia sensor measurements of the oxygen release reveal that the crystal growth rate is limited by liquid-phase diffusion; the properties of the gaseous environment, which were previously assumed to be decisive, are almost insignificant. Consequently, large and stoichiometric single crystals of VO₂ can be obtained at lower temperatures and gas purities than usually applied. These results signify the role of gas-liquid diffusion in crystal growth and will simplify future research on VO₂ and related materials for applications in ultrafast electronics and thermal energy management.

DOI: [10.1103/PhysRevResearch.5.013028](https://doi.org/10.1103/PhysRevResearch.5.013028)

I. INTRODUCTION

Vanadium dioxide (VO₂) is a strongly correlated transition metal oxide with a notable first-order insulator-to-metal phase transition at a temperature of around 68° C [1]. At this temperature, which can be controlled by strain [2], pressure [3], or stoichiometry [4], the crystal structure changes from a monoclinic $P2_1/c$ low-temperature phase to a tetragonal $P4_2/mnm$ high-temperature phase within a time of only hundreds of femtoseconds [5–11]. The electrical, optical, thermal, and magnetic properties transform substantially as well [1,4,12–15]. Theoretical physics is challenged by the strong interplay and coupling between the electronic, magnetic, and vibrational subsystems [5,16], and experimental physics only begins to capture the combined electronic/atomic reaction path at fundamental resolutions in space and time [6–10]. In applied physics, VO₂ single crystals, VO₂ nanoparticles, or VO₂-doped materials are ideal as ultrafast and temperature-dependent switches for electric current, infrared light, and heat conduction. In particular, the substantial modulation of its near-infrared transparency makes VO₂ a promising material for next-generation energy-saving smart windows that are reflective for thermal radiation in summer but transparent at colder times [17–19].

Consequently, VO₂ has been and is widely examined by the entire arsenal of modern measurement techniques [1–19]. However, most of these investigations are performed with

rather inhomogeneous thin films, nanoparticles, or different kinds of compositions [13–17], although the microscopic geometry, substrate material, degree of polycrystallinity, and related imperfections are well known to influence the macroscopic observations, concealing the basic physics of the pure material. Hence, researchers strive to investigate single-crystalline VO₂ as well, but large high-quality crystals with good surface flatness, stoichiometry, and monocrystallinity are difficult to obtain.

A common method for growing macroscopic VO₂ crystals is the thermal decomposition of vanadium pentoxide (V₂O₅) [4,20–22]. Basically, V₂O₅ is heated up in an oxygen-free environment and decomposes into solid VO₂ and gaseous O₂ which is continuously removed by a flow of inert gas. Crystal growth under such conditions is usually described with a thermodynamic theory by MacChesney and Guggenheim based on Gibbs phase rule [4]. This theory suggests that the growth rate at a given temperature is limited by the equilibrium oxygen partial pressure of the reaction in the gaseous phase. This partial pressure is reported to be only ~10⁻¹⁴ at 800° C or ~10⁻⁸ at 1000° C [4,20,23]. Consequently, large reaction temperatures and very pure inert gases are usually applied, making the growth a complicated experiment. Alternatively, a high-temperature centrifuge can be applied to remove residual V₂O₅ during crystal growth [24].

In this work, we report the growth of mm-sized, stoichiometric, VO₂ single-crystals at O₂ partial pressures that are several orders of magnitude higher, and therefore much easier to achieve, than the values reported in previous experiments [4,20,23]. Time-resolved zirconia sensor measurements of the amount and speed of oxygen release as a function of temperature and V₂O₅ educt mass reveal that not the vapor pressure of the V₂O₅-VO₂-O₂ system but rather the diffusion rate of O₂ through the liquid V₂O₅ is the essential factor for the limited growth speed and nice crystal formation. Consequently, crystals can be grown in less complex setups, using less pure

^{*}These authors contributed equally to this work.

[†]peter.baum@uni-konstanz.de

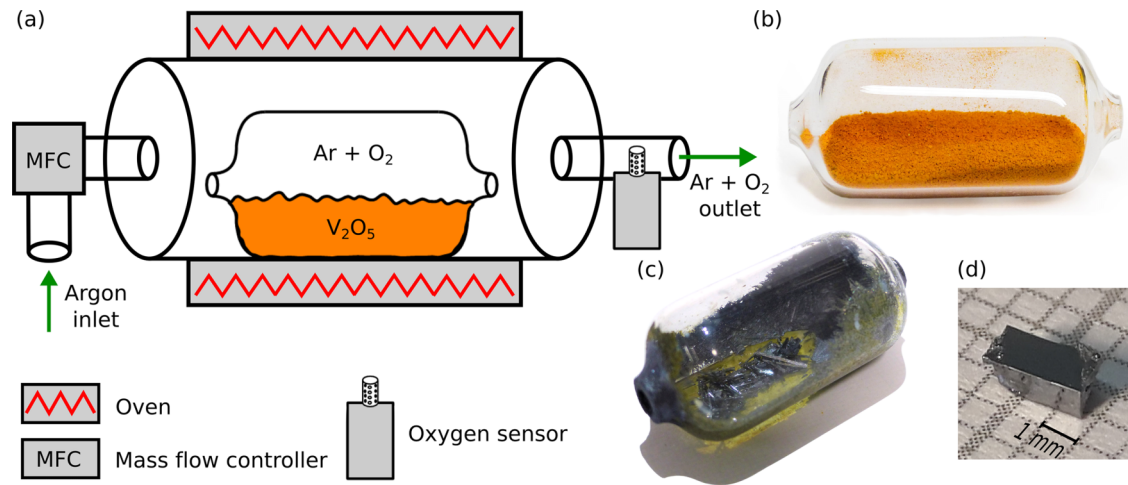


FIG. 1. Experimental setup. (a) Sketch of the growth setup with oxygen detection. (b) Ampoule with V_2O_5 powder before the growth process; length ~ 50 mm, diameter ~ 22 mm. (c) Ampoule with VO_2 crystals after the growth process. (d) Typical VO_2 single-crystal as grown in this liquid-diffusion setup. The surfaces are optically flat without any processing.

inert gasses and lower temperatures at optimum growth rates for single-crystal formation. Characterization of our crystals by x-ray diffraction, resistivity measurements, and energy dispersive x-ray spectroscopy reveals the purity of the material and thus establishes the benefits of a liquid-diffusion-limited growth process for high-quality VO_2 materials.

II. EXPERIMENTAL SETUP

Figure 1(a) depicts the experimental setup. A quartz ampoule is filled with about 2 g of V_2O_5 powder [Fig. 1(b)] with a purity of $\geq 99.6\%$ (Sigma-Aldrich 221899) and placed inside a tube furnace. The system is constantly flooded at a rate of 250 ml/min with argon 5.0, regulated by a mass flow controller. The oxygen content in the outlet is monitored by a zirconia sensor (PZA-MC25-P, Pewatron). The furnace is heated up to its working temperature (typically $975\text{--}1000^\circ\text{C}$) over a period of 12 h. Afterwards, the temperature is kept constant until the reaction is over, evident by the sensor-detected stop of oxygen release. The ampoule is now filled with black, needlelike VO_2 single crystals [see Fig. 1(c)] with heights and widths of a few mm and optically flat surfaces [see Fig. 1(d)]. The length of the crystals reaches up to several cm, limited by the size of the ampoule.

III. DYNAMICS OF THE GROWTH PROCESS

To better understand the growth mechanism, we use the oxygen sensor as a real-time monitor of the reaction dynamics. Fig. 2 shows the oxygen emission rate $\dot{N}_{O_2}(t)$ and the temperature development inside the oven during a typical growth process with a maximum temperature of 975°C and a V_2O_5 educt mass of 2.0 g.

We see three characteristic peaks of particularly strong oxygen emission. The first peak at ~ 8 h (peak 1) is relatively small and appears when the oven reaches a temperature of 690°C , the melting point of V_2O_5 . Oxygen impurities trapped in hollow spaces inside the V_2O_5 powder are released at this point. Afterwards, the emission rate increases along with the

temperature and culminates into a second peak at $t \approx 12$ h. Then the emission rate declines until the complete crucible reaches the process temperature of 975°C at $t_0 \approx 13.3$ h (dotted line). After this equilibration point, thermodynamic growth theory [4] would predict a constant evaporation rate of oxygen out of the system. However, we find a continuously increasing emission rate, initially slow but then accelerating (dashed line), until the reaction ends with a final emission maximum (peak 3) at $t \approx 33$ h.

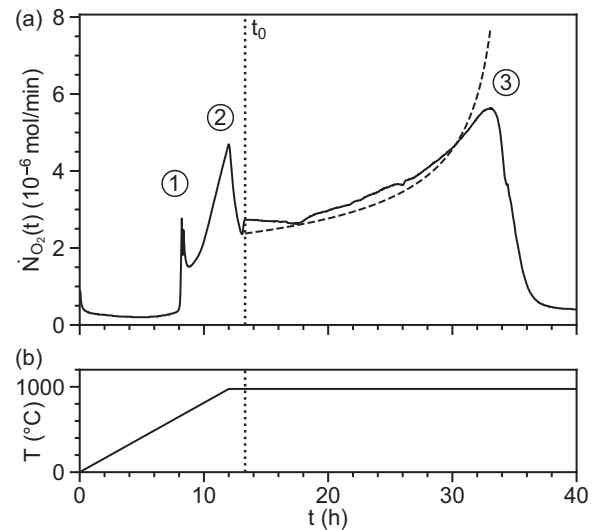


FIG. 2. Macroscopic influences on the crystal growth. (a) Development of the oxygen emission rate $\dot{N}_{O_2}(t)$. Peak 1 can be ascribed to the melting point of V_2O_5 . At peak 2, at 12.0 h, the maximum oven temperature of 975°C is reached. From here on, convection streams, which so far enhanced the oxygen transport, slowly vanish until the system reaches thermal equilibrium at 13.3 h (dotted line). The increasing behavior afterwards, until peak 3, is caused by the change of the diffusion distance during the process via Eq. (4) (dashed curve). The properties of the inert gas are almost irrelevant. (b) Oven temperature as a function of time.

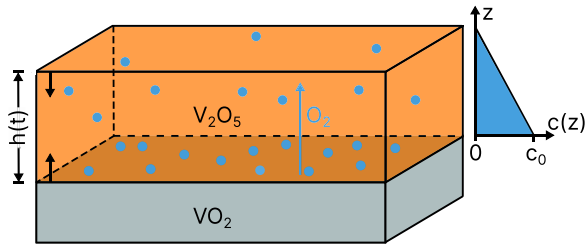


FIG. 3. Model system describing the growth process. Solid VO_2 (grey) at the bottom of the ampoule is covered by liquid V_2O_5 (orange). Thermal decomposition of V_2O_5 causes a constant oxygen concentration c_0 at the VO_2 - V_2O_5 interface (dark orange) and a continuously decreasing diffusion distance $h(t)$. In the stationary limit, the oxygen concentration $c(z)$ decreases linearly with distance z inside the V_2O_5 melt (blue inset).

IV. INTERPRETATION

To explain these observations, we drop the assumption of a rate limitation by the oxygen partial pressure in the gas atmosphere [4,20,23] and rather assume that the reaction speed is limited by the rate with which the generated oxygen can be removed out of the liquid V_2O_5 . In this picture, not the vapor pressure of O_2 at a given temperature [4] but rather the diffusion rate of O_2 within liquid V_2O_5 is the limiting factor for the reaction. Because solid VO_2 is denser than liquid V_2O_5 , the crystals start growing at the bottom of the crucible. The oxygen emerging there dissolves into the melt. The overall reaction speed is determined by the rate with which oxygen is transported through the enclosing liquid V_2O_5 into the atmosphere, where it is removed out of the system.

With these considerations, almost all the experimental observations can be explained. Shortly after the initial release of

trapped impurities in peak 1 at the melting point (690°C), V_2O_5 immediately starts with its decomposition according to $2\text{V}_2\text{O}_5 \rightarrow 4\text{VO}_2 + \text{O}_2$. While the oven temperature is still increasing, the bottom of the ampoule is warmer than the top, and convection enhances the initial oxygen transport out of the melt. Consequently, a burst is observed in the oxygen emission rate (peak 2). When the maximum temperature is reached at $t = 12$ h, the convection slowly vanishes, causing the measured drop of oxygen emission until the system is in thermal equilibrium around $t_0 \approx 13.3$ h. From this point on, there is no more convection. At the bottom of the ampoule, VO_2 crystals are now growing steadily and slowly at a rate that is limited by the ability of oxygen to diffuse upwards through the ambient liquid V_2O_5 to the surface, where it is removed.

As more and more V_2O_5 gets decomposed, the liquid V_2O_5 level drops while the growing VO_2 crystals start stacking at the bottom of the crucible. Consequently, the diffusion distance decreases and induces a stronger gradient of oxygen concentration between the bottom and the top. The diffusion rate increases until all V_2O_5 is used up and the process comes to an end (peak 3).

V. ANALYTICAL DIFFUSION MODEL

We support this explanation by an analytical description that can, despite its simplicity, reproduce almost all of the measurement results. Fig. 3 depicts the model geometry. The ampoule is approximated as a cuboid with a cross sectional area A in which a layer of solid VO_2 (grey) coexists with a layer of liquid V_2O_5 (orange) with a time-dependent height $h(t)$. The oxygen concentration $c_0 = c(z = 0)$ on the VO_2 - V_2O_5 interface (dark orange) is constant and the oxygen concentration in the gas phase is $c(z \geq h) \approx 0$. Gas-phase

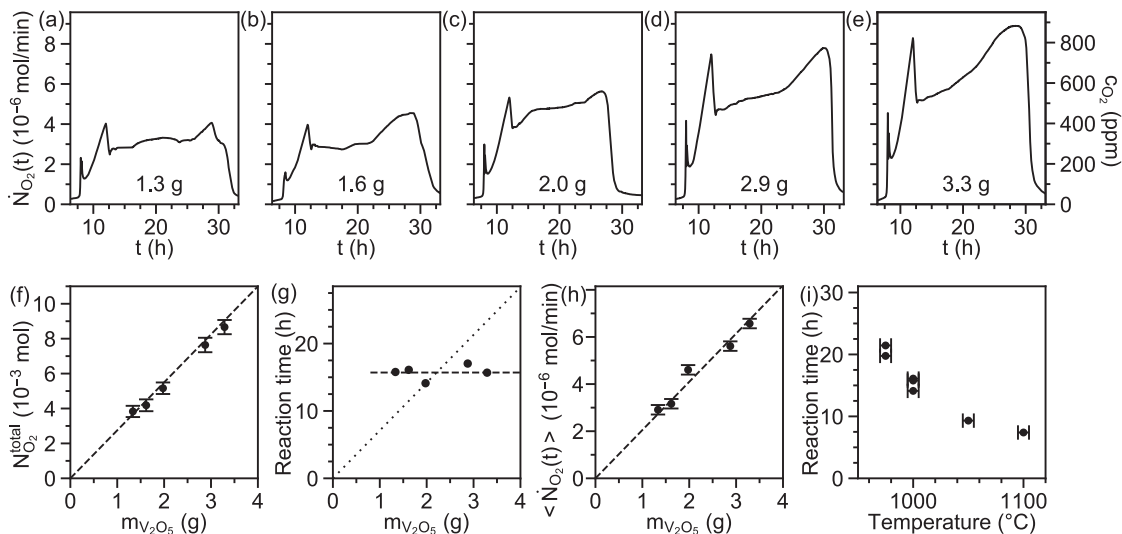


FIG. 4. Mass and temperature dependence of the growth process. (a)–(e) Measurements of the oxygen emission rate $\dot{N}_{\text{O}_2}(t)$ for increasing V_2O_5 educt mass. The three distinct emission peaks appear always at almost the same times. (f) Total amount of released oxygen as a function of the V_2O_5 educt mass. The dashed line denotes the expectation for a complete stoichiometric $2\text{V}_2\text{O}_5 \rightarrow 4\text{VO}_2 + \text{O}_2$ reaction. (g) Measured reaction time as a function of the V_2O_5 educt mass. The dotted line is the expected behavior according to thermodynamic theory [4]; the dashed line is a guide to the eye. (h) Average O_2 emission rate as a function of the V_2O_5 educt mass. The dashed line is a linear fit. (i) Measured total reaction time for different equilibrium temperatures.

dynamics and partial pressure effects of the atmosphere are completely excluded from the model. Using Fick's first law, we obtain

$$j = \frac{\dot{N}_{O_2}(t)}{A} = -D \frac{\partial c(z)}{\partial z}, \quad (1)$$

where j is the diffusion flux through the VO_2 - V_2O_5 interface (rate of O_2 molecules per area A), D is the diffusion constant, and $c(z)$ is the oxygen concentration in the melt. Since the process takes place on long time scales, the diffusion is assumed to happen in the stationary limit, which means $\frac{\partial c(z)}{\partial z} = \frac{-c_0}{h(t)}$. We obtain

$$\dot{N}_{O_2}(t) = \frac{A}{h(t)} D c_0. \quad (2)$$

We see that the oxygen emission rate is proportional to the ratio of the surface A and the diffusion distance $h(t)$. Considering the stoichiometry of the reaction ($2V_2O_5 \rightarrow 4VO_2 + O_2$), we express $h(t)$ as

$$h(N_{O_2}(t)) = \frac{V_{V_2O_5}^{\text{molec}}}{A} N_{V_2O_5}(t) = \frac{V_{V_2O_5}^{\text{molec}}}{A} (N_{V_2O_5}(t_0) - 2N_{O_2}(t)), \quad (3)$$

where $V_{V_2O_5}^{\text{molec}}$ is the V_2O_5 molecular volume and $N_{V_2O_5}(t_0)$ is the number of V_2O_5 molecules at the begin of the diffusion process. With these considerations, the solution of the differential Eq. (2) becomes

$$\dot{N}_{O_2}(t) = \frac{\lambda}{\sqrt{-4\lambda t + N_{V_2O_5}(t_0)^2}}, \quad (4)$$

with $\lambda = A^2 D c_0 / V_{V_2O_5}^{\text{molec}}$.

We want to compare Eq. (4) now with our measurements. $N_{V_2O_5}(t_0)$ can be easily determined from the V_2O_5 educt mass and the amount of prereleased oxygen, which is given by the integral over the oxygen emission curve in Fig. 2(a) between $t = 0$ and t_0 , excluding peak 1. Furthermore, the total amount of released oxygen must be the same in experiment and theory. This boundary condition allows us to calculate $D c_0 = 1.8 \times 10^{16} \text{ m}^{-1} \text{ s}^{-1}$.

Figure 2(a) depicts the results as a dashed line. Without any fitted parameters, we see an agreement to the experiment; in particular, we reproduce the measured characteristic increase of the reaction speed towards the end of the process. These results indicate that liquid diffusion and not gas-phase dynamics is indeed the essential and limiting factor for the speed and dynamics of VO_2 formation.

VI. SYSTEMATIC INVESTIGATION

Going back to the experiment, we next investigate the physics of the growth process as a function of the amount of initial V_2O_5 . All other parameters are kept the same; the equilibrium temperature is 1000°C . Figs. 4(a)–4(e) show the measured time-dependent oxygen emission rate $\dot{N}_{O_2}(t)$ for different V_2O_5 educt masses. We see in all traces the three prominent emission peaks as explained above (a first one from impurities released at the melting point, a second peak from convection-assisted oxygen transport, and a third peak at the end of the reaction due to a decreasing diffusion distance).

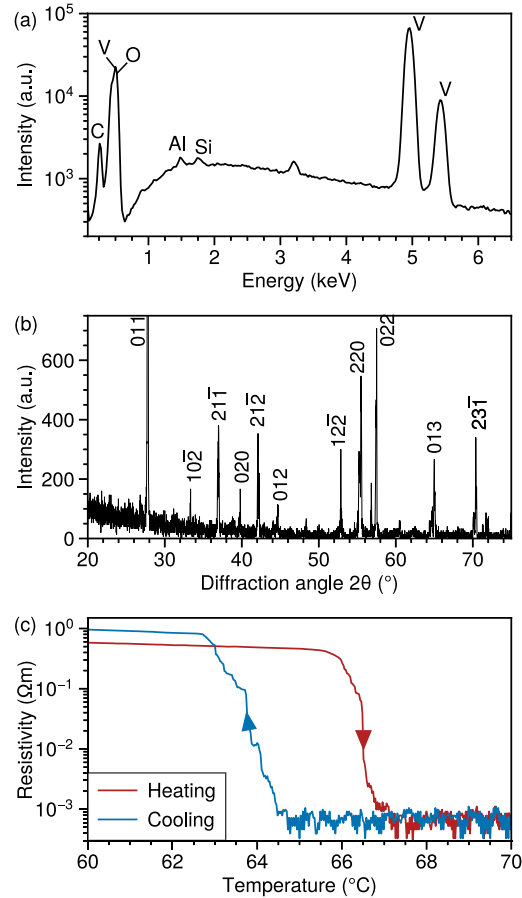


FIG. 5. Spectroscopic characterization of the VO_2 crystals. (a) EDX spectrum of the VO_2 crystals. The peaks are labeled with the corresponding elements. The unlabeled peaks are escape peaks. (b) Room temperature powder XRD spectrum of the VO_2 crystals, recorded by a coupled 2θ - ω scan. The peaks are labeled with the corresponding Miller indices. (c) Metal-to-insulator transition and its hysteresis curve. Measured electrical resistivity as a function of temperature during warmup (red) and cooldown (blue).

Interestingly, the end of the crystal growth occurs in all cases at almost the same time ($t \approx 30 \text{ h}$), even if almost three times more material is converted.

Figure 2(f) shows the total amount of released oxygen, obtained by integrating over the measured traces of Figs. 2(a)–2(e). The dashed line denotes the amount of oxygen that is expected from a perfectly stoichiometric $2V_2O_5 \rightarrow 4VO_2 + O_2$ reaction. We see that all V_2O_5 is perfectly converted into VO_2 in all cases. Figure 4(g) shows the measured duration of the reaction (after t_0) as a function of the educt mass. In contrast to the expectation from thermodynamic theory [4], in which the reaction time should be directly proportional to the educt mass since only a constant rate of oxygen can be transported out of the system, we measure a nearly constant duration of the reaction that is almost independent of the educt mass (dashed line). Figure 4(h) shows the mean O_2 emission rate, averaged over the period where the sample is in thermal equilibrium (between t_0 and peak 3). We see a reaction speed that is proportional to the reaction mass, again in contrast to the thermodynamic model [4] in which the reaction

TABLE I. Lattice parameters of the VO_2 crystals at room temperature.

a (Å)	b (Å)	c (Å)	α (°)	β (°)	γ (°)
5.75	4.53	5.39	90.0	122.6	90.0

equilibrium would cause a constant partial pressure in the system as long as some educt is left, leading to a constant emission rate, independent of initial educt mass. Figure 2(i) shows the measured reaction time as a function of temperature. We observe an increase in reaction speed at higher temperatures, which we explain by temperature-dependent changes of the diffusion constant of O_2 in liquid V_2O_5 . In the experiments using reaction temperatures above 1000°C we obtain about three times smaller VO_2 crystals than at $975\text{--}1000^\circ\text{C}$. At too high temperatures, the diffusion and thereby the reaction rate are too fast for an orderly crystal growth. In future experiments, an active control of the reaction speed as a function of time and progress, for example via temperature regulations with feedback from the oxygen sensor, is expected to produce even better crystals than so far obtained, in shorter time.

VII. SAMPLE CHARACTERIZATION

The atomic composition of the VO_2 crystals is analyzed by energy dispersive x-ray spectroscopy (EDX). Figure 5(a) shows the EDX spectrum of the VO_2 crystals. It exhibits clear maxima for vanadium and oxygen, accompanied by slight amounts of carbon, silicon, and aluminum. The aluminum peak could originate from the housing of the measuring device and may not necessarily be related to our materials. Carbon and silicon can be attributed to the typical impurities in rather cheap and imperfectly refined V_2O_5 powders such as used in our experiments. We also performed EDX on several spots in a cut through one of our VO_2 crystals. The results are identical to the surface scans shown in Fig. 5(a), indicating a uniform crystal composition.

The crystal structure of our samples was analyzed by powder x-ray diffraction (XRD) at room temperature with a coupled $2\theta\text{--}\omega$ scan. The recorded diffraction data is shown in Fig. 5(b). All peaks match the values reported in literature [25,26]. The lattice parameters extracted from the XRD spectrum are listed in Table I.

To examine the insulator-to-metal phase transition and its hysteresis, we measure the temperature-dependent electrical

resistivity during a heating and cooling cycle. The crystals are contacted with silver-paste and the resistance is recorded between room temperature and 70°C inside a nonconductive water bath. The results are shown in Fig. 5(c). We clearly see the insulator-to-metal phase transition from a low temperature semiconductorlike behavior with high resistivity at low temperatures into a metallic high-temperature phase at a transition temperature of $T_i \approx 65^\circ\text{C}$. The resistivity changes by more than three orders of magnitude and exhibits a hysteresis width of about 2.5°C . The steepness of the individual transitions is limited by the rather quick temperature changes of the experiment. After the phase transition cycle, the final resistivity (blue) is slightly higher than before (red), probably due to the formation of microfractures [4]. Fig. 6 shows a series of scanning electron microscopy images of the as-grown, unprocessed crystal surfaces [see Fig. 1(d)] at different magnifications. We see almost perfectly flat areas down to length scales of tens of nanometers. In all three data sets of Fig. 6, dust particles or a crack were searched for properly focusing the electron beam onto the otherwise featureless surface morphology. By inspecting crystals from one of our earlier growth runs, we see no considerable surface degeneration after storage of the crystals under ambient laboratory conditions for more than one year. In optical pump-probe experiments, to be published elsewhere, we successfully observed a fully reversible phase transition cycle for more than 10^7 times.

VIII. CONCLUSION AND OUTLOOK

In summary, these results show that high-quality VO_2 single-crystals can be obtained by a crystallization process in which the growth rate is limited by liquid diffusion. In this way, the slow and ordered growth at the growing crystal surfaces is self-stabilizing; if a certain part on the surface grows too rapidly, the local oxygen concentration increases, limiting the growth. In contrast to earlier belief, the properties of the gaseous environment are almost insignificant for the growth. The oxygen partial pressure that is necessary for the growth can exceed 800 ppm [see Fig. 4(e)] which is more than a thousand times higher, and therefore easier to achieve, than previously reported [4,20,23]. Consequently, substantially simpler apparatuses and materials are sufficient for producing high-quality single crystals for applications and research. The idea to measure oxygen emission provides valuable feedback for understanding and optimizing the growth rate and thereby the number, morphology, and macroscopic properties of the crystals. In particular, we expect that a

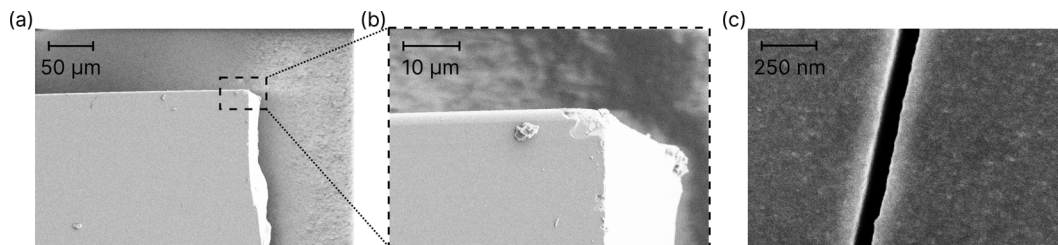


FIG. 6. Scanning electron microscopy data. (a) Corner of a VO_2 crystal. (b) The same corner for higher magnification. (c) Nanometer-resolution data around a crack (black). Black-white colors refer to measured secondary electron counts, normalized.

slowdown of the heating around the point of convection (peak 2) will substantially reduce the number of seeds and therefore facilitate the growth of bigger crystals at no substantial increase of the total reaction time. Also, the reaction can be stopped before a total conversion in case that, for example, the final VO₂ crystals shall remain within a V₂O₅ layer in order to avoid the condensation of impurities onto the surfaces. More generally, the ability to control the speed of a crystallization process by utilizing liquid-phase diffusion in combination with a sensor that instantaneously measures the reaction rate seems to provide a general and versatile route towards high-quality crystal growth at an always optimum reaction rate. In principle, the findings reported in our work should apply to any reaction in which a liquid converts into a gas and a solid, providing general principles for related growths of even more intricate materials than VO₂ for modern condensed-matter physics research.

All data needed to evaluate the conclusions in the paper are present in the paper.

ACKNOWLEDGMENTS

We thank C. Müller for manufacturing the quartz ampoules and M. Hagner for support with the growth apparatus and EDX measurements. We acknowledge financial support by the Evangelisches Studienwerk e.V., the Deutsche Forschungsgemeinschaft through Sonderforschungsbereich SFB 1432, and the Dr. K. H. Eberle Stiftung.

P.B. conceived the experiment. N.S. built the setup for the crystal growth and optimized the process. N.S. and D.K. conceived the diffusion theory. N.S. and R.H. performed the XRD analysis. N.S. performed the EDX and resistance analysis. All authors wrote the manuscript.

The authors declare no competing interests.

-
- [1] F. J. Morin, Oxides Which Show a Metal-to-Insulator Transition at the Neel Temperature, *Phys. Rev. Lett.* **3**, 34 (1959).
- [2] B. Hu, Y. Ding, W. Chen, D. Kulkarni, Y. Shen, V. V. Tsukruk, and Z. L. Wang, External-strain induced insulating phase transition in VO₂ nanobeams and its application as flexible strain sensor, *Adv Mater.* **22**, 5134 (2010).
- [3] Y. Chen, S. Zhang, F. Ke, C. Ko, S. Lee, K. Liu, B. Chen, J. W. Ager, R. Jeanloz, V. Eyert, and J. Wu, Pressure-temperature phase diagram of vanadium dioxide, *Nano Lett.* **17**, 2512 (2017).
- [4] J. MacChesney and H. Guggenheim, Growth and electrical properties of vanadium dioxide single crystals containing selected impurity ions, *J. Phys. Chem. Solids* **30**, 225 (1969).
- [5] D. Wegkamp and J. Stähler, Ultrafast dynamics during the photoinduced phase transition in VO₂, *Prog. Surf. Sci.* **90**, 464 (2015).
- [6] A. Cavalleri, C. Tóth, C. W. Siders, J. A. Squier, F. Ráksi, P. Forget, and J. C. Kieffer, Femtosecond Structural Dynamics in VO₂ During an Ultrafast Solid-Solid Phase Transition, *Phys. Rev. Lett.* **87**, 237401 (2001).
- [7] P. Baum, D. S. Yang, and A. H. Zewail, 4D visualization of transitional structures in phase transformations by electron diffraction, *Science* **318**, 788 (2007).
- [8] A. Pashkin, C. Kübler, H. Ehrke, R. Lopez, A. Halabica, R. F. Haglund, R. Huber, and A. Leitenstorfer, Ultrafast insulator-metal phase transition in VO₂ studied by multiterahertz spectroscopy, *Phys. Rev. B* **83**, 195120 (2011).
- [9] V. R. Morrison, R. P. Chatelain, K. L. Tiwari, A. Hendaoui, A. Bruhács, M. Chaker, and B. J. Siwick, A photoinduced metal-like phase of monoclinic VO₂ revealed by ultrafast electron diffraction, *Science* **346**, 445 (2014).
- [10] D. S. Yang, P. Baum, and A. H. Zewail, Ultrafast electron crystallography of the cooperative reaction path in vanadium dioxide, *Struct. Dyn.* **3**, 034304 (2016).
- [11] L. Vidas, D. Schick, E. Martinez, D. Perez-Salinas, A. Ramos-Álvarez, S. Cichy, S. Battle-Porro, A. S. Johnson, K. A. Hallman, R. F. Haglund, and S. Wall, Does VO₂ Host a Transient Monoclinic Metallic Phase?, *Phys. Rev. X* **10**, 031047 (2020).
- [12] J. H. Park, J. M. Coy, T. S. Kasirga, C. Huang, Z. Fei, S. Hunter, and D. H. Cobden, Measurement of a solid-state triple point at the metal-insulator transition in VO₂, *Nature (London)* **500**, 431 (2013).
- [13] J. A. Ramirez-Rincon, C. L. Gomez-Heredia, A. Corvisier, J. Ordonez-Miranda, T. Girardeau, F. Paumier, C. Champeaux, F. Dumas-Bouchiat, Y. Ezzahri, K. Joulain, O. Ares, and J. J. Alvarado-Gil, Thermal hysteresis measurement of the VO₂ dielectric function for its metal-insulator transition by visible-IR ellipsometry, *J. Appl. Phys.* **124**, 195102 (2018).
- [14] R. Zhang, Q. S. Fu, C. Y. Yin, C. L. Li, X. H. Chen, G. Y. Qian, C. L. Lu, S. L. Yuan, X. J. Zhao, and H. Z. Tao, Understanding of metal-insulator transition in VO₂ based on experimental and theoretical investigations of magnetic features, *Sci. Rep.* **8**, 17093 (2018).
- [15] C. L. Gomez-Heredia, J. A. Ramirez-Rincon, D. Bhardwaj, P. Rajasekar, I. J. Tadeo, J. L. Cervantes-Lopez, J. Ordonez-Miranda, O. Ares, A. M. Umarji, J. Drevillon, K. Joulain, Y. Ezzahri, and J. J. Alvarado-Gil, Measurement of the hysteretic thermal properties of W-doped and undoped nanocrystalline powders of VO₂, *Sci. Rep.* **9**, 14687 (2019).
- [16] K. Okazaki, S. Sugai, Y. Muraoka, and Z. Hiroi, Role of electron-electron and electron-phonon interaction effects in the optical conductivity of VO₂, *Phys. Rev. B* **73**, 165116 (2006).
- [17] Y. Cui, Y. Ke, C. Liu, Z. Chen, N. Wang, L. Zhang, Y. Zhou, S. Wang, Y. Gao, and Y. Long, Thermochromic VO₂ for energy-efficient smart windows, *Joule* **2**, 1707 (2018).
- [18] S. Wang, T. Jiang, Y. Meng, R. Yang, G. Tan, and Y. Long, Scalable thermochromic smart windows with passive radiative cooling regulation, *Science* **374**, 1501 (2021).
- [19] K. Tang, K. Dong, J. Li, M. P. Gordon, F. G. Reichertz, H. Kim, Y. Rho, Q. Wang, C.-Y. Lin, C. P. Grigoropoulos, A. Javey, J. J. Urban, J. Yao, R. Levinson, and J. Wu, Temperature-adaptive radiative coating for all-season household thermal regulation, *Science* **374**, 1504 (2021).
- [20] S. Aramaki and R. Roy, Single-crystal growth of VO₂ by isothermal flux-evaporation, *J. Mater. Sci.* **3**, 643 (1968).
- [21] S. Wall, S. Yang, L. Vidas, M. Chollet, J. M. Glowina, M. Kozina, T. Katayama, T. Henighan, M. Jiang, T. A. Miller, D. A. Reis, L. A. Boatner, O. Delaire, and M. Trigo, Ultrafast

- disordering of vanadium dimers in photoexcited VO₂, [Science](#) **362**, 572 (2018).
- [22] H. Sasaki and A. Watanabe, A new growing method for VO₂ single crystals, [J. Phys. Soc. Jpn.](#) **19**, 1748 (1964).
- [23] J. B. MacChesney, J. F. Potter, and H. J. Guggenheim, Preparation and properties of vanadium dioxide films, [J. Electrochem. Soc.](#) **115**, 52 (1968).
- [24] T. Kong, M. W. Masters, S. L. Bud'ko, and P. C. Canfield, Physical properties of VO_{1-x}Ti_xO₂ (0 < x < 0.187) single crystals, [APL Mater.](#) **3**, 041502 (2015).
- [25] Crystallography open database (COD): An open-access collection of crystal structures, COD ID: 9009089.
- [26] R. W. G. Wyckoff, *Crystal Structures*, 2nd ed. (Wiley, New York, 1963).